Hindawi
International Journal of Antennas and Propagation
Volume 2017, Article ID 5924157, 7 pages
https://doi.org/10.1155/2017/5924157

Research Article

The Strip-Ground Rectangular Patch Antenna

Yiying Wang and Yinghua Lu

School of Electrical Engineering, Beijing University of Posts and Telecommunications, Beijing 100876, China

Correspondence should be addressed to Yiying Wang; yiying520@126.com

Received 27 February 2017; Revised 14 April 2017; Accepted 20 April 2017; Published 5 June 2017

Academic Editor: Xiulong Bao

To imitate the broken situation of the conductive threads of the wearable antenna, a strip-ground design of rectangular patch antenna with the conventional substrate is presented to investigate the change of the antenna performance, where the ground is sliced along its *E*-plane. The strips are symmetrical along the center line of the width of the patch, and the gap ratio of the gap to the solid ground varies with the change of gaps. The conventional patch antenna is used as a reference for comparison with the stripe-ground antennas. And the effect of the coaxial cable, the changes of the impedance, and the cross-polarization of the antenna are investigated. Several antenna prototypes are fabricated and their measured results are in good agreement with the simulations. These results show that the gaps change the performance of the strip-ground antennas, but they can work well if the gap ratio is less than 1 : 4.

1. Introduction

In recent years, the wearable antenna is being studied to be used in the Body Area Network (BAN) and Personnel Area Network (PAN). Among these different antenna types, the microstrip topology antenna [1–5] has attracted a lot of attentions because it has a low profile, low cost, lightweight, simple installation, and conformability to planar and nonplanar surfaces [6, 7]. However, the patch and the ground of the textile antenna are exposed outside and hence may be destroyed because of the aging or be cut or may break abruptly, and so forth, so that the performance will change. This broken situation gives us a chance to investigate the corresponding performance of antenna and in how much damage degree can still the antenna work, which is represented by the gap ratio of the gap to the solid ground in this paper.

At present, there are two known ways to fabricate the wearable antenna: one is the inject-printed technique [5] and the other is conductive thread [1–4]. It is clear that the inject-printed layer is very similar to that of the solid one. And for the woven conductive threads, they almost connect to each other, and even if there exists the gap, they are tightly coupled. These lead to the textile looking like a solid one so that it is reasonable to imitate it by the conventional design. Besides, the conventional antenna can be made into textile one using the methods mentioned in [1–5, 8]. Therefore, in this paper, the broken situation is imitated by slicing the ground plane of the conventional patch antenna.

The patch antennas have been sliced into the meshed ones for different applications [9–12]. It is impossible to print the metal on glass if it exceeds a few millimeters across in the shaping/lamination process, so the authors designed the meshed patch antennas to overcome the difficulties [9], where the meshed ground caused the back radiation. The meshed patch antennas were also used in the tiny satellite application [10–12] to satisfy the requirements of both the solar cells and the communication. However, the meshed method did not cut off the current distribution but made it more complicated. In contrast, there were some researches on cutting off the current distributions of the patch [13, 14] but they were excited by the slots, which were different from coaxial feeding methods.

As we know, there exists a current loop between the patch and ground plane when the antenna is excited. Obviously, if the patch is truncated perpendicular to the current direction, that is the y-axis direction shown in Figure 1, the effective current patch will shorten and the resonance will shift to the higher frequency. But if the method mentioned in [13, 14] is adopted, the feeding method has to be changed because the

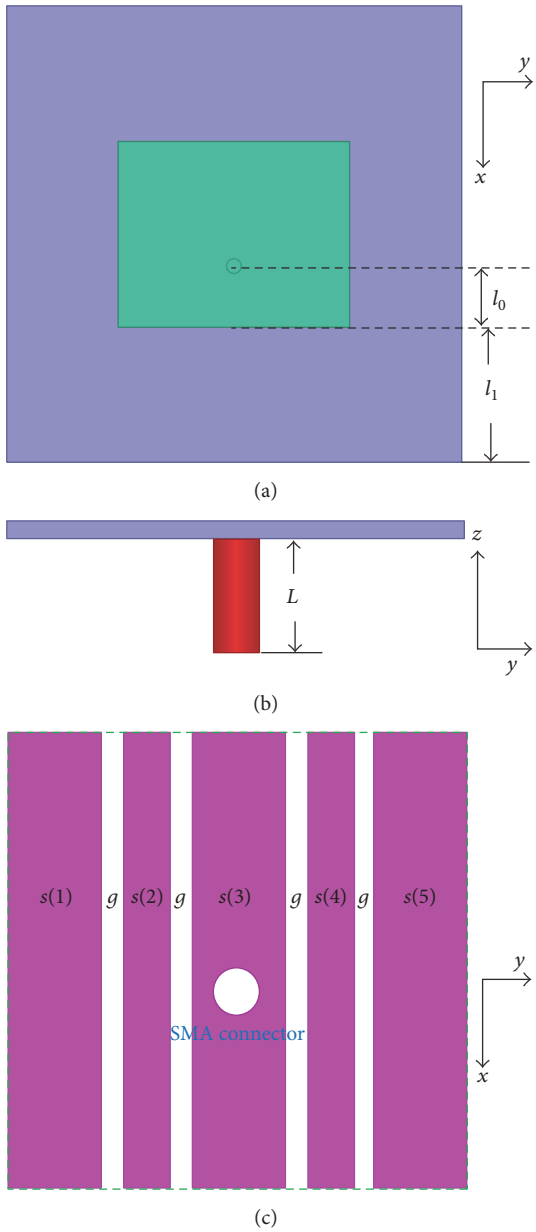

FIGURE 1: The overall view of the strip-ground antenna. (a) Front view of the patch. (b) Side view of the model. (c) Front view of the sliced ground plane.

coaxial probe cannot excite the pieces simultaneously. On the other hand, the resonance of the finite-ground patch antenna, comparing with the infinite one, is affected little if the sizes on all sides of the ground are $\lambda_0/20$ larger than those of the patch [15]. In other words, the area beyond this range affects the antenna little. Thus, in this paper, the sliced area is not limited to the above-mentioned range. Besides, the ground is sliced across its E-plane and not only is one gap adopted to investigate the performance, but also the effect with one gap can be estimated by simplifying this complicated situation.

Here, the solid ground plane is assumed to be sliced into 5 strips which they are symmetrical on current direction as shown in Figure 1(c). From this structure, it is clear that if the antenna is excited, there will be conductive currents on the patch and the middle strip, then generating the coupling currents among the strips and the patch as well as between the neighboring strips. Changing the sizes of the gaps will change the corresponding couplings and the gap ratio of the gap to the solid ground as well, and then the performance is changed simultaneously. Additionally, the coaxial cable couples the power through the gaps so that its effect is also investigated in this paper.

2. Antenna Design

The conventional patch antenna is designed as a benchmark to be compared with the strip-ground antenna prototypes. And the solid ground of the conventional antenna is sliced into 5 strips while the patch is held. The substrate is Wangling's F4BM220, where the height h is 1.50 mm, the relative permittivity ε_r is 2.20, and the loss tangent tan δ is 0.001. The originally intended resonant frequency is 5.80 GHz which is used to calculate the length and the width of the patch [6, 7]. The approximate values of the corresponding length and width are 16.4 mm and 20.5 mm, respectively. And the dimension of the ground plane is 40 mm × 40 mm. The feeding point is defined by using the parametric method of HFSS software.

Figure 1 shows the overall view of the strip-ground patch antenna, their corresponding coordinates, and the parameters investigated in this design. Figure 1(a) shows the front view of the patch which is the same as the conventional one, the side view of the simulated model is shown in Figure 1(b), and Figure 1(c) is of the sliced ground plane, where the dashed green line is the boundary of the ground plane of the conventional patch antenna and the blank circle is the position of the SMA connector. Among these parameters, length l_1, which is the distance from the boundary of the substrate to the nearest edge of the patch, is a constant. In other words, the position of the patch remains the same. Nevertheless, distance l_0, which comes from the low edge of the patch to the center of the feeding probe, the length of the coaxial cable in the simulations, and the gaps g and the widths $s(i)$ $(i = 1, 2, 3, 4, 5)$ of the strips are variables. However, in this paper, the widths of the inner three strips are kept as constants but adjust the widths of the gaps and the outer two strips.

The antenna prototypes, including the conventional antenna and three strip-ground antennas with different gaps, are fabricated. And they are measured in the anechoic chamber, as shown in Figure 2. The following analyses are based on the comparisons of the simulated and the measured results.

2.1. Effect of the Coaxial Cable on the Antenna Design. As we know the current distribution on the ground plane of the conventional patch antenna mainly concentrates just under the patch, as shown in Figure 3, which is the vector current distribution of the resonant frequency 5.61 GHz at 0 degrees. Here, the practical resonance shifts to the lower from the

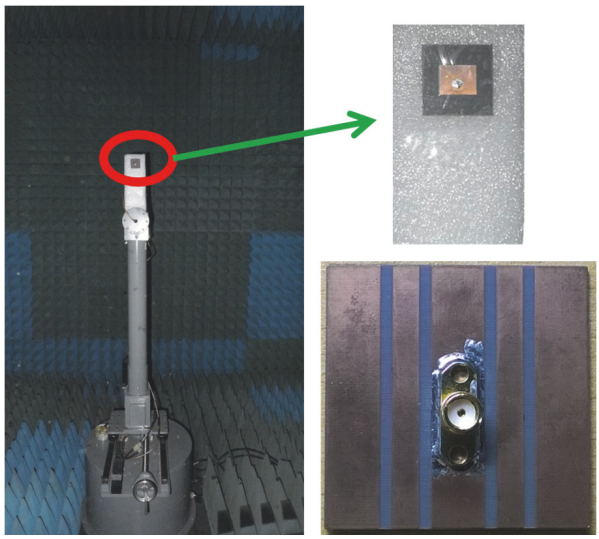

Figure 2: One measured prototype in the anechoic chamber.

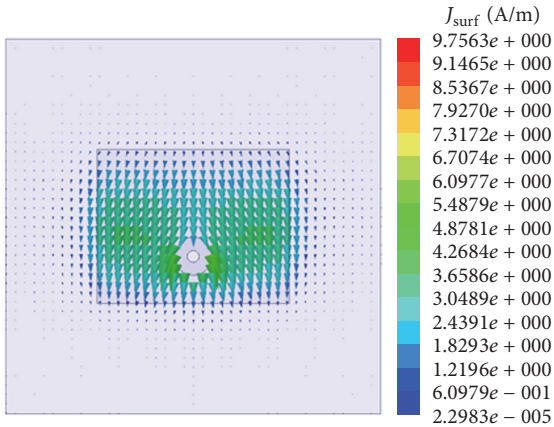

Figure 3: The vector current distribution of 0 degrees on the solid ground plane of the conventional patch antenna.

aforementioned 5.80 GHz. However, after slicing the ground, parts of the current will disappear and leave the gap to couple the power to the coaxial cable so that it becomes a key factor to affect the antenna performance and be studied. The effect is studied from two aspects, comparing the simulated and measured reflection coefficients of different gaps to lead to the effect of the cable and then setting the different height of the simulated cable for one fixed-gap antenna to study its effect.

As shown in Figure 1(c), the strips are symmetrical on the width direction and have different widths, that is, $s(1) = s(5)$, $s(2) = s(4)$, and $s(3)$. However, the gaps are the same. In these designs, the gaps increase gradually in order to study the change of antenna performance caused by the couplings among patch and strips. The simulated and measured reflection coefficients of different gaps and strips are shown in Figure 4, where the corresponding sizes are listed in Table 1 and the antennas with the one gap width 1 mm, 2 mm, and 4 mm are represented by Antennas A, B, and C, respectively. Then the corresponding simulated heights of

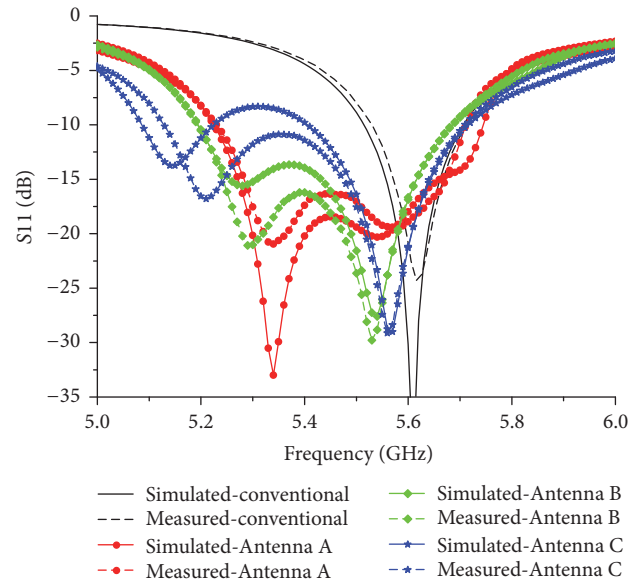

Figure 4: Comparisons of reflection coefficients for different gaps.

the cable in the models are shown in Figure 4, where the height L is shown in Figure 1(b).

In Figure 4, the simulated and measured results are represented by the solid and the dashed lines, respectively. And the black lines without markers present the results of the conventional antenna; the red lines with the circle markers, the green lines with the diamond markers, and the blue lines with the star markers correspond to Antennas A, B, and C, respectively. From the comparisons, it is known that the simulated results agree well with the measurements for both the resonances and bandwidths. There exist two resonant frequencies for the strip-ground antennas, and they shift to the lower one compared with the conventional one. However, the simulated result of Antenna C shows the dual-band characteristic, while the measured result does not show it. That is because the effect of the solder and the SMA position cannot be simulated so well, resulting in the notion that the measurement has a wider bandwidth.

The effects of the cables in the models of the aforementioned simulations in Figure 4 are considered. Additionally, the grounding in the simulations is taken into account by connecting the cable with the radiation boundary. Moreover, the simulated height L depends on the corresponding gaps which also determine its lower resonance. That is because when the strip-ground antenna is excited, the patch and middle strip are filled with currents and consequently couple the other strips. This process causes that the higher resonance is affected little which can be found in Figure 4, even though the gaps are different, but the lower resonance, which is generated by parasitic inductances capacitors, shifts to the lower frequency. Their relationships are shown in Figure 5, where the black circle line represents the ratio of gaps to the space wavelength λ_0 at 5.61 GHz and the red star line is that of height to λ_0. For conventional antenna design, the effect of the cable is not an important consideration because the ground plane is large enough to prevent the couplings.

Table 1: Detailed dimensions of the different antennas (unit: mm).

Types	Variables			
	g	$s(1)/s(5)$	$s(2)/s(4)$	$s(3)$
Antenna A	1	10	4	8
Antenna B	2	8	4	8
Antenna C	4	4	4	8

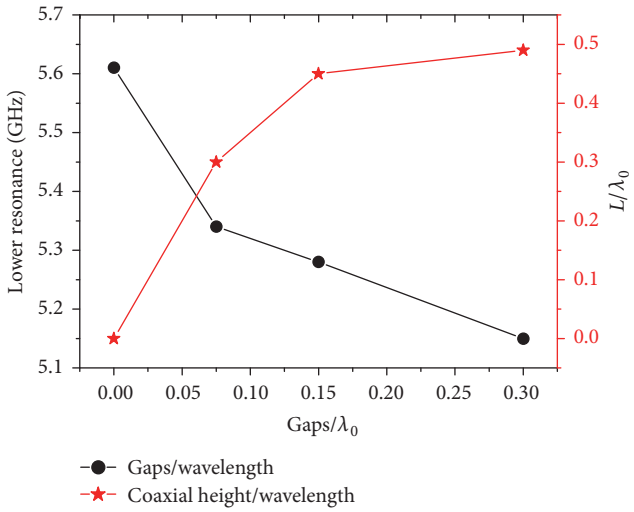

Figure 5: The simulated height L and gaps versus lower resonance.

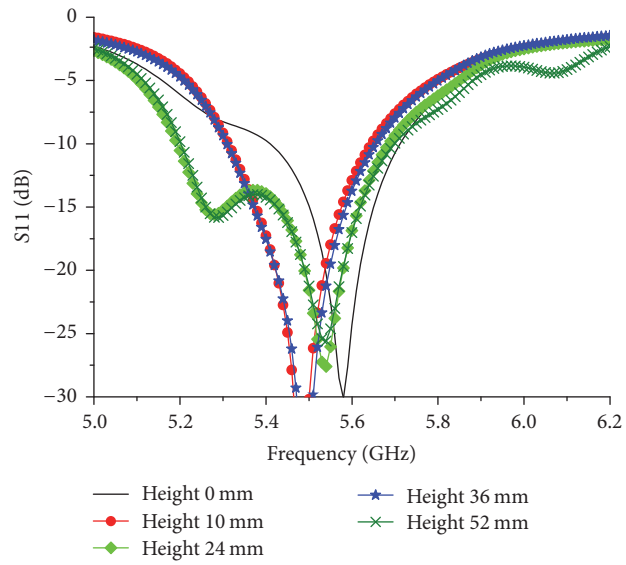

Figure 6: Parametric study of the cable height in the simulations.

Thus, both its height and gap are 0 mm. However, for the strip-ground antennas, the cable height increases as the gaps increase, but when the gaps are larger than 8 mm ($0.15\lambda_0$) the increase becomes slow, such that the height is 24 mm ($0.45\lambda_0$) for Antenna B and 26 mm ($0.49\lambda_0$) for Antenna C, while it is 16 mm ($0.30\lambda_0$) for Antenna A compared to the conventional one. In other words, if the gaps are large enough, the height of the simulated cable will approach to a constant. This also applies to the resonance. The lower resonance shifts to the lower frequency and the change becomes small as the increase of the gaps.

Depending on the above analysis, the other topic on the effect of the cable height to a fixed-gap antenna is also studied. Here, Antenna B is taken as an example. The corresponding simulated results of different heights are shown in Figure 6, which just presents 5 representative results. The black line without markers, the red line with circles, the green line with diamonds, the blue line with stars, and the olive line with crosses are the simulated results of heights 0 mm, 10 mm, 24 mm, 36 mm, and 52 mm, respectively. From the figure, it is found that the results at the heights 0 mm, 10 mm, and 36 mm do not have the two resonant frequencies, while the other two have them. The bandwidth of the 0 mm height is almost the same as bandwidths of both 10 mm and 36 mm and less than those of both 24 mm and 52 mm, though the resonances shift to the lower. These results show that the effect of the cable is so obvious that it not only changes the resonance but also changes the bandwidth. And it causes the dual band of the antenna. Furthermore, $S11$s are periodic because the result of the length 10 mm is the same as that of 36 mm and also suits the results of 24 mm and 52 mm. From these two groups data, the period is found to be about $\lambda_0/2$. And the above-mentioned simulated height used to be compared with the measurement is also 24 mm, which is also about $0.45\lambda_0$. Actually, the height is not so sensitive to the result; if the height enlarges to 26 mm ($\lambda_0/2$), $S11$ changes little. Thus, it is concluded that the shortest height range of the cable in the simulation is from $0.45\lambda_0$ to $0.5\lambda_0$.

2.2. Change of the Impedance. According to the formulas reported in [6, 7], the effective permittivity of the patch is calculated on the assumption that the ground plane is large enough. Hence, it will be changed after slicing so that the effective width changes and the effective impedance changes consequently. The corresponding changes of the feeding length, which is the sum of the lengths l_0 and l_1, are shown in Table 2, where l_0 and l_1 are shown in Figure 1(a), and here just show the change of the length l_0 because l_1 is the constant 11.80 mm. These results are gotten by using the parametric methods in the HFSS software. Table 2 shows that the feedings are shifted closer to the center of the patch compared with that of the conventional antenna, but the shift is just 0.40 mm, which is not so great. However, the feeding positions for the three different gaps are the same; in other words, the impedance is not changed even if the gaps have changed if the width listed in Table 1 of the feeding strip, which is put in

Table 2: Feeding position of different antennas (unit: mm).

Variables	Types			
	Conventional	Antenna A	Antenna B	Antenna C
l_0	5.00	5.40	5.40	5.40

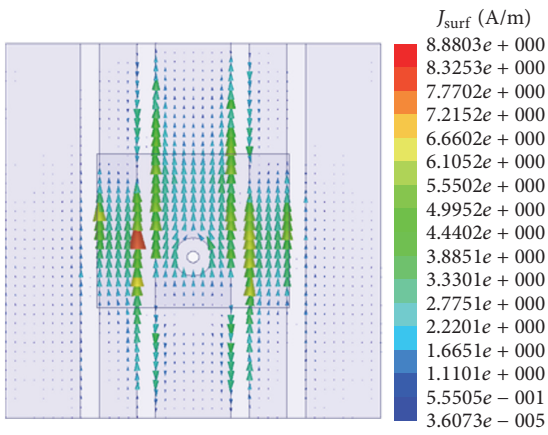

Figure 7: Vector current distribution of 0 degrees at 5.54 GHz.

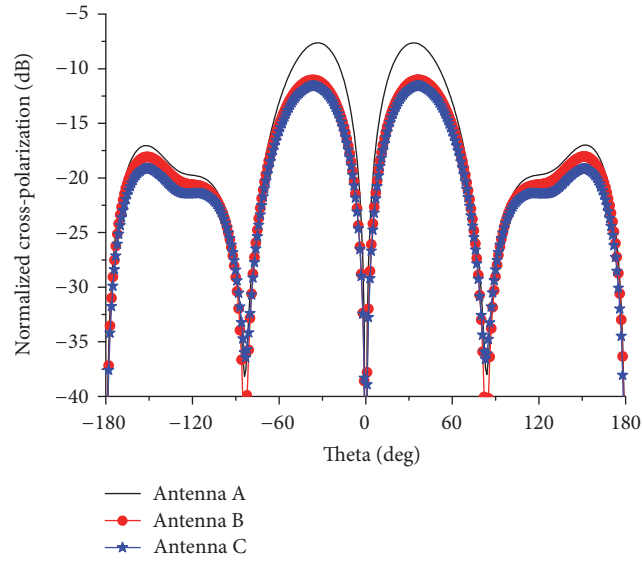

Figure 8: Comparisons of normalized cross-polarization at higher resonance.

the middle and connected with the SMA connector, remains the constant.

2.3. Back Radiation and Cross-Polarization. After slicing, there remain 4 gaps on the ground and this leads to the current distribution becoming complicated and maybe affect the back radiation and cross-polarization, which are discussed in this section. Figure 7 shows the vector current distribution of 0 degrees of Antenna B at its higher simulated resonant frequency 5.54 GHz. Compared with the current distribution shown in Figure 3, it is found that the phase difference of the current between the strip-ground antenna and the conventional antenna is 180 degrees. However, this does not affect the patch as the radiator because the current on the patch also reverses. In addition, the current density distribution surrounds the area of the patch which is similar to that of the conventional antenna and it is also mainly affected by the patch, whereas, beyond the projection of the patch, the currents have opposite directions at the ends of the middle strip though they are a small proportion of power, and the current of middle strip couples to the neighboring two strips and these coupled currents consequently couple the outside two strips, resulting in their directions being opposite. Consequently, the back radiation is affected little.

The strip-ground antenna destroys the current distribution continuity of the solid ground resulting in intervals existing when the current flows between the patch and striped ground. Consequently, the cross-polarization of the *E*-plane is destroyed but that of *H*-plane is not affected because of the symmetry of the geometry. Figure 8 shows the normalized cross-polarization of *E*-plane for the three antennas, where they are normalized by using their own copolarization at the higher resonant frequency, that is, 5.54 GHz, 5.54 GHz, and 5.57 GHz for Antennas A, B, and C, respectively. The black line represents the result of Antenna A, Antenna B is indicated by the red line with circles, and the blue line with stars belongs to Antenna C. From this figure, it is known that the obvious changes are focused on the range from −90 to 90 degrees and Antenna A has the biggest cross-polarization. That is because the small gaps generate great couplings among strips which destroy the current more seriously.

3. Result Analysis and Discussion

The above sections have stated the design dimension of the antenna, the method to slice the ground, and the analysis of the influencing factors. Besides, the measured results of four antenna prototypes were also mentioned to verify the simulated results. Here, the results of Antenna B are analyzed further.

3.1. Reflection Coefficient and Gap Ratio. The comparisons of simulated and measured results for different gaps are shown in Figure 3. They agree well with each other for both Antennas A and B, but the measured result is better than the simulated for Antenna C because the effect of the solder and the SMA position cannot be simulated so exactly. To solder conveniently in these designs, the center strip width listed in Table 1 is a constant 8 mm, which is a little wider than the practical width 5.58 mm of the SMA arm, and the widths of the two neighboring strips beside the center are also kept as constants. Then, the gaps are changed, while the widths of the outermost two strips are shortened to study the performance. As mentioned above, the power mainly concentrates on the area of the patch so that this shifting method can achieve the goal of investigating the effect of the gap ratio to the antenna. From the above analysis, a conclusion is gotten that if the gap ratio is more than 1 : 4, the strip-ground antenna will

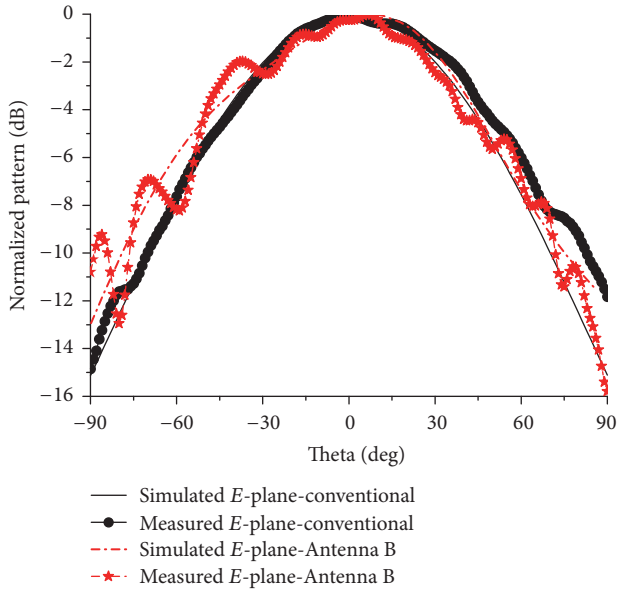

Figure 9: Comparisons of E-plane patterns for the conventional antenna and Antenna B.

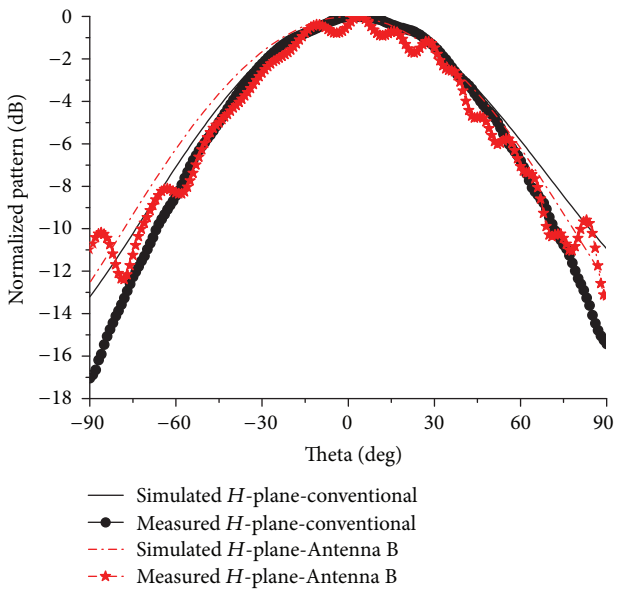

Figure 10: Comparisons of H-plane patterns for the conventional antenna and Antenna B.

have dual band, and the welding, which affects the antenna performance, should be taken care of well.

The effect of the cable to the reflection coefficient was also analyzed as shown in Figure 6. The simulated results show that the height of the cable should be set to a correct range, or the effect will not appear. That is to say, the cable causes the dual band for the strip-ground antenna and generates the lower resonance and the wider bandwidth.

3.2. Pattern and Realized Gain. The previous paragraph mentioned the effect of the cable to the reflection coefficient which caused the lower resonant frequency and widened the bandwidth. Thus, only the comparisons of patterns for both the conventional antenna and Antenna B at their higher resonances are shown to verify the antenna design; the comparisons of simulated and measured E-plane and H-plane patterns are shown in Figures 9 and 10, respectively. In these two figures, the simulated and measured results of the conventional antenna are represented by the black solid lines without and with circle markers, respectively, while the red dashed dot lines without and with star markers belong to those of Antenna B. From the comparisons, it is known that they agree well with each other for both the simulated E- and H-planes to their corresponding measurements, and the beamwidths are almost not changed for Antenna B compared with those of the conventional antenna. That is to say, the radiation is barely affected by the slicing.

The simulated and measured realized gains are shown in Figure 11, where the conventional antenna is taken into account to be compared. The black and red colors represent the simulated and measured results, respectively. And the short dashed lines are the results of the conventional antenna, while the solid lines belong to those of sliced antenna. Besides, the lines with and without markers indicate the

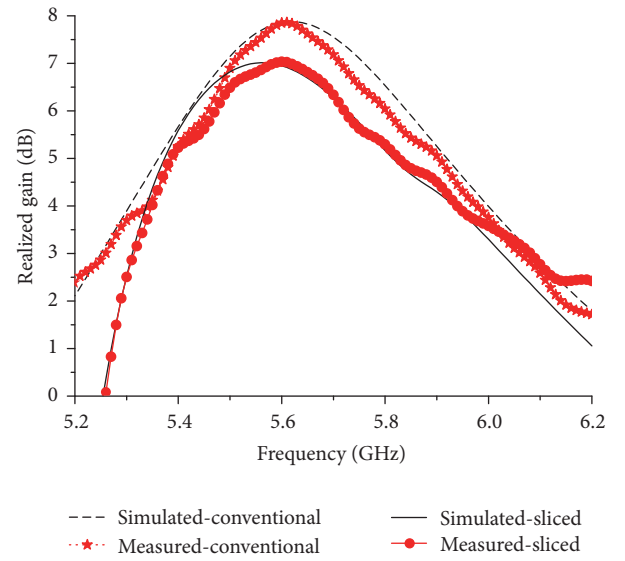

Figure 11: Realized gains versus frequency of the conventional antenna and Antenna B.

measured and simulated results, respectively; that is, the star line is of the conventional antenna while the circle line suggests the sliced one. These results show that the simulated results have good agreements with those corresponding measurements. Combining the results shown in Figure 3, the detailed result comparisons are listed in Table 3, which just shows the measured results of the conventional antenna because it is almost the same as the simulated one. It shows that the simulated results are also almost the same as those measured for Antenna B. The realized gain of Antenna B is a little less than that of the conventional one, and the difference is 0.82 dB.

Table 3: Comparisons between the conventional antenna and Antenna B.

Types	Variables			
	f_0 (GHz)	Impedance BW/Range (GHz)	G_{max} (dB)	Gain BW/range (GHz)
Conventional	5.61	0.18 5.53–5.71	7.86	0.57 5.38–5.95
Strip-simu	5.28 & 5.54	0.49 5.19–5.68	7.01	0.59 5.34–5.93
Strip-meas	5.29 & 5.53	0.48 5.20–5.68	7.04	0.59 5.35–5.94

Combining the analysis of its reflection coefficient, it is found that though the resonant frequency and bandwidth are affected greatly, its realized gain is affected little. This explains that the back radiation is affected little in another way, or the realized gain will be smaller. And the realized gain at the lower simulated resonance 5.28 GHz is just 1.54 dB and smaller than that of the conventional one at this frequency, which is another way to verify that this resonant frequency is induced by the involvement of the coaxial cable.

4. Conclusion

In this paper, we introduced the design of a strip-ground rectangular patch antenna, where the solid ground was sliced into 5 strips and changed the gap ratio by changing the size of the gaps and the outermost two strips, while the inner three strips were kept as the constant. The effect factors were analyzed, including the height of the cable, the gap ratio, and the feeding point. The conventional and three strip-ground antenna prototypes were fabricated. The simulated results agreed well with the measured ones, and the comparisons were taken between the conventional and the strip-ground antennas. The analysis showed that if the gap ratio of the gap to the solid ground is less than 1 : 4, the strip-ground antenna can work well, though the cross-polarization becomes greater than that of the conventional one. These results indicate this technology can be used in the wearable antenna design.

Conflicts of Interest

The authors declare that there are no conflicts of interest regarding the publication of this paper.

References

[1] E. F. Sundarsingh, S. Velan, M. Kanagasabai, A. K. Sarma, C. Raviteja, and M. G. N. Alsath, "Polygon-shaped slotted dual-band antenna for wearable applications," *IEEE Antennas and Wireless Propagation Letters*, vol. 13, pp. 611–614, 2014.

[2] N. Ehteshami, V. Sathi, and M. Ehteshami, "Experimental investigation of a circularly polarised flexible polymer/composite microstrip antenna for wearable applications," *IET Microwaves, Antennas and Propagation*, vol. 6, no. 15, pp. 1681–1686, 2012.

[3] C. Hertleer, H. Rogier, L. Vallozzi, and L. Van Langenhove, "A textile antenna for off-body communication integrated into protective clothing for firefighters," *IEEE Transactions on Antennas and Propagation*, vol. 57, no. 7, pp. 919–925, 2009.

[4] P. B. Samal, P. J. Soh, and G. A. E. Vandenbosch, "UWB all-textile antenna with full ground plane for off-body WBAN communications," *IEEE Transactions on Antennas and Propagation*, vol. 62, no. 1, pp. 102–108, 2014.

[5] W. G. Whittow, A. Chauraya, J. C. Vardaxoglou et al., "Inkjet-printed microstrip patch antennas realized on textile for wearable applications," *IEEE Antennas and Wireless Propagation Letters*, vol. 13, pp. 71–74, 2014.

[6] C. A. Balanis, *Antenna Theory Analysis and Design*, John Wiley & Sons Inc, New Jersey, NJ, USA, 3rd edition, 2005.

[7] R. Garg, B. Prakash, I. Bahl, and A. Ittipiboon, *Microstrip Antenna Design Handbook: Artech House*, Boston, Mass, USA, 2001.

[8] K. Koski, A. Vena, L. Sydanheimo, L. Ukkonen, and Y. Rahmat-Samii, "Design and implementation of electro-textile ground planes for wearable UHF RFID patch tag antennas," *IEEE Antennas and Wireless Propagation Letters*, vol. 12, pp. 964–967, 2013.

[9] G. Clasen and R. Langley, "Meshed patch antennas," *IEEE Transactions on Antennas and Propagation*, vol. 52, no. 6, pp. 1412–1416, 2004.

[10] S. Sheikh, "Circularly Polarized Meshed Patch Antenna," *IEEE Antennas and Wireless Propagation Letters*, vol. 15, pp. 352–355, 2016.

[11] T. W. Turpin and R. Baktur, "Meshed patch antennas integrated on solar cells," *IEEE Antennas and Wireless Propagation Letters*, vol. 8, pp. 693–696, 2009.

[12] T. Yasin and R. Baktur, "Circularly polarized meshed patch antenna for small satellite application," *IEEE Antennas and Wireless Propagation Letters*, vol. 12, pp. 1057–1060, 2013.

[13] Y. Jia, Y. Liu, and S. Gong, "Slot-coupled broadband patch antenna," *Electronics Letters*, vol. 51, no. 6, pp. 445–447, 2015.

[14] W. Liu, Z. N. Chen, and X. Qing, "Metamaterial-Based Low-Profile Broadband Aperture-Coupled Grid-Slotted Patch Antenna," *IEEE Transactions on Antennas and Propagation*, vol. 63, no. 7, pp. 3325–3329, 2015.

[15] E. Lier and K. R. Jakobsen, "Rectangular Microstrip Patch Antennas with Infinite and Finite Ground Plane Dimensions," *IEEE Transactions on Antennas and Propagation*, vol. 31, no. 6, pp. 978–984, 1983.